Research on Flexural Strengthening Efficiency of Hybrid Fiber Reinforced Polymer Laminates in RC Beams: Experimental and Numerical Investigation

Asjad Javed[1], Dr. M. Adil Khan[2], Abdul Rehman Ghumman[3], Waqas Aziz[4], Engr. Baitullah Khan Kibzai[5], Kashif Daud[6], Samiullah Memon[7], Abdul Haq[8,9] *

[1] *Communication and Works Department, Punjab, Pakistan*
[2] *Resident Engineer (RE), National Engineering Services Pakistan (NESPAK), Lahore, Pakistan*
[3] *Communication and Department, Pakistan*
[4] *University of Southern Punjab Multan, Pakistan*
[5] *Senior Engineer, PCSIR, Karachi, Pakistan*
[6] *Khyber Pakhtunkhwa Urban Mobility Authority, Transport & Mass Transit Department, Khyber Pakhtunkhwa, Pakistan*
[7] *Mehran University of Engineering and Technology, Jamshoro, Sindh, Pakistan*
[8] *School of Civil Engineering Southeast university, 211189, Nanjing, China,*
[9] *Advance Ocean Institute of Southeast University Nantong, China.*

*Corresponding Author: Abdul Haq
Email: 223227020@seu.edu.cn

Abstract
This study investigates the flexural strengthening efficiency of reinforced concrete (RC) beams using externally bonded Hybrid Fiber Reinforced Polymer (HFRP) laminates, addressing the critical need for robust rehabilitation strategies in aging infrastructure. To utilize a comprehensive dual approach, the research combines experimental testing with advanced numerical simulations. Five RC beams, including a control specimen and four strengthened with varying HFRP laminate thicknesses and configurations (including end-anchorage), were subjected to four-point bending tests. The experimental results demonstrate significant enhancements in load-carrying capacity, with the optimally strengthened beam (HB-3) achieve a 198% increase and the anchored specimen (HB-5) reached a 214% increase in ultimate load compared to the control beam. These findings highlight the presence of an optimal laminate thickness, beyond which excessive material can lead to premature interfacial debonding, as observed in HB-4. Complement the experimental work, a non-linear finite element model was developed using LS-DYNA, incorporate the Continuous Surface Cap Model (MAT_159) for concrete and detailed contact definitions for the HFRP-concrete interface. The numerical simulations accurately reproduced the experimental load-deflection responses, crack progression, and failure modes, with ultimate load predictions deviating by less than 5%. This strong correlation validates the model's reliability for predicting the behavior of HFRP-strengthened RC beams. The study concludes that HFRP laminates offer a highly effective solution for flexural retrofitting, particularly when optimized for thickness and supplemented with adequate anchorage, thereby contributing to more durable and resilient civil infrastructure.
Keywords: Flexural strength, RC beams, Composite materials, HFRP, Flexural strength

1. Introduction

The structural integrity and longevity of existing civil infrastructure represent a critical concern for engineers and policymakers worldwide. As reinforced concrete (RC) structures age, they are frequently subjected to increased

service loads, environmental degradation, and seismic vulnerabilities that necessitate effective rehabilitation and retrofitting strategies (Palacios-Munoz et al., 2019). The traditional methods of structural strengthening, such as the application of steel plates or concrete jacketing has encounter limitations related to corrosion susceptibility and labor-intensive installation processes (Fayed et al., 2023; Shi, 2025). Subsequently, the development and implementation of advanced composite materials have emerged as a transformative approach in structural engineering. Fiber-reinforced polymer (FRP) composites, considered by their high strength-to-weight ratio (Diniță et al., 2023), excellent corrosion resistance, and versatility have gained significant prominence since the 1980s as a superior alternative for enhancing the performance of deficient RC components (Sakar et al., 2014).

Among the various types of FRP materials, Glass Fiber Reinforced Polymer (GFRP), Carbon Fiber Reinforced Polymer (CFRP), and Aramid Fiber Reinforced Polymer (AFRP) are the most commonly utilized. As CFRP offers exceptional stiffness and strength, its high cost and brittle failure mode can be restrictive (Pawlak et al., 2022). Conversely, GFRP is cost-effective and possesses high deformability but lacks the tensile modulus of carbon fibers (Attari et al., 2012). AFRP provides a balanced profile with superior chemical resistance and toughness (Ahmed et al., 2021). Recent advancements in material science have led to the concept of "hybridization," where different fiber types are combined within a single resin matrix to create Hybrid Fiber Reinforced Polymer (HFRP) laminates (Zhang et al., 2025). This strategy aims to develop the cooperative effects of multiple fibers such as the stiffness of carbon, the ductility of glass, and the impact resistance of aramid to overcome the inherent weaknesses of individual fiber types and optimize the overall mechanical response of the strengthening system. Comparative studies have shown that while single-fiber FRP systems typically increase bearing capacity by 20% as hybrid configurations can achieve significantly higher efficiencies (Yuvaraj et al., 2023). For instance, recent literature indicates that optimized hybrid FRP sheets can increase the maximum bearing capacity of RC specimens by up to 30.2% in historical structures (B. Lin et al., 2024), and in some cases, specific HFRP configurations have demonstrated an ultimate load carrying capacity increase of up to 170% compared to unstrengthen control beams (Hawileh et al., 2014).

Despite the creation of FRP strengthening techniques, numerous critical gaps remain in the understanding of hybrid systems. Specifically, the efficiency of flexural strengthening using HFRP laminates is highly sensitive to the configuration of the hybrid layers, the thickness of the laminate, and the integrity of the bond at the concrete-composite interface (Jafari et al., 2025; Luo et al., 2024; Silva & Meddaikar, 2020). This study addresses two research question: (1) To what extent can the flexural capacity and ductility of RC beams be optimized through the application of HFRP laminates? (2) How do variables such as laminate thickness and end-anchorage systems influence the failure mechanisms and overall strengthening efficiency? Furthermore, the study seeks to determine if there exists an optimal threshold for laminate thickness beyond which the gains in load-carrying capacity are diminished by premature interfacial debonding. The primary objective of this research is to evaluate the flexural strengthening efficiency of HFRP laminates in RC beams through a dual approach involving experimental testing and numerical validation. To achieve this, the following specific objectives were established:

1. To design and fabricate various HFRP laminate configurations (Carbon-Aramid, Glass-Aramid, and Cross-woven balanced) and characterize their mechanical properties.
2. To conduct experimental four-point bending tests on a series of RC beams, including a control specimen and beams strengthened with varying thicknesses of HFRP laminates.
3. To develop a robust non-linear finite element model using LS-DYNA to simulate the structural response, crack propagation, and failure modes of the strengthened beams.

The scope of this investigation is focused on the flexural behavior of medium-scale RC beams with a consistent reinforcement ratio of 0.82%, designed to ensure an under-reinforced failure mode. The study specifically examines the performance of externally bonded HFRP laminates applied to the beam soffit. Five different strengthening schemes are evaluated from single-layer applications to double-layer configurations and the inclusion of mechanical end-anchorage. The experimental program utilizes a four-point bending configuration over an effective span of 2400 mm. The numerical scope involves the application of the Continuous Surface Cap Model (CSCM) in LS-DYNA to capture the complex non-linear interactions between the concrete, steel reinforcement, and the composite laminates, focusing on ultimate load, mid-span deflection, and energy absorption.

Moreover, the significance of this research lies in its potential to refine the design guidelines for the use of hybrid composites in infrastructure rehabilitation. By demonstrating that HFRP laminates can achieve substantial increases in load-carrying capacity that reach up to 214% in some. This performance exceeds typical benchmarks found in recent research, where average ductility losses of approximately 42% are reported for hybrid-strengthened specimens (Tefera et al., 2024). Moreover, the identification of an "optimum laminate thickness" is a crucial finding for practitioners, as it warns against the inefficient use of excessive materials that may trigger brittle debonding failures. The successful validation of the LS-DYNA numerical model offers a sophisticated framework for engineers to simulate and optimize strengthening interventions without the need for exhaustive physical testing. The reliability of such models is well-documented, with advanced finite element simulations typically maintaining deviation rates within 3% to 5% for ultimate load predictions (Al-Saawani et al., 2022). Ultimately, this work contributes to the development of more sustainable and resilient infrastructure provided that a cost-effective and high-performance solution for extending the service life of existing RC structures. The methodology adopted in this study follows a rigorous scientific workflow. It begins with the selection of materials, where a M30 grade concrete mix and Fe500 grade steel reinforcement are utilized to cast the beam specimens. The HFRP laminates are fabricated using a controlled hand lay-up process, integrating carbon, glass, and aramid fibers in specific architectures. The strengthening procedure involves precise surface preparation of the concrete soffit through mechanical roughening and cleaning, followed by the application of a two-component epoxy adhesive system.

2. Materials and Experimental Procedure

2.1 The Concrete-Mix

The RC beam specimens were cast using a normal-weight concrete mix designed to achieve a characteristic compressive strength corresponding to M30 grade. The mix proportions were determined in accordance with IS 10262:2019 and IS 456:2000 standards. A target mean strength of 38 MPa at 28 days was adopted during the design stage to ensure adequate structural performance. Ready-mix concrete was employed to maintain batch-to-batch consistency and minimize variability in mechanical properties. The statistical analysis of compressive strength results indicated a standard deviation of 1.002 MPa and a coefficient of variation of 0.03 to demonstrate controlled production quality. To verify the mechanical characteristics of the concrete, standard cube, prism, and cylindrical specimens were cast alongside the beam specimens. After 28 days of curing, the average compressive strength of cubes was 36 MPa, the flexural strength of prisms was 4.77 MPa, and the split tensile strength of cylinders was approximately 4.0 MPa. The detailed mix composition per cubic meter of concrete is presented in **Table 1**, which summarizes the quantities of water, cement, fine aggregate, coarse aggregate, superplasticizer, and the adopted water-cement ratio (Bureau of Indian Standards, 2007, 2019).

Table 1. Mix proportions for M30 grade concrete (per m³)

Material (kg)	Quantity
Water	144
Cement	360
Fine aggregate	752
Coarse aggregate	1196
Superplasticizer	3.6
Water–cement ratio	0.44

2.2 Steel Reinforcement

High-yield strength deformed (HYSD) reinforcing bars of Fe500 grade were used as both longitudinal and transverse reinforcement in the RC beams. To determine the actual mechanical properties of the steel, tensile tests were conducted on reinforcing bar coupons with nominal diameters of 10 mm and 12 mm (Odusote et al., 2019). The experimentally measured yield strength and ultimate tensile strength values are summarized in **Table 2.** The test results show that the

reinforcing bars exhibit a typical elastic plastic stress-strain response, characterized by a distinct yield point followed by strain hardening up to failure. These measured properties were used in the subsequent analysis to ensure that the numerical and experimental evaluations reflect the actual material behavior of the reinforcement.

Table 2. Mechanical properties of reinforcing steel

Ultimate Tensile Strength (MPa)	Diameter (mm)	Yield Strength (MPa)
~410 to 550	10	~250
~410 to 550	12	~250

2.3 Hybrid Fiber Reinforced Polymer (HFRP) Laminates

The strengthening system consisted of HFRP laminates fabricated using different combinations of carbon, glass, and aramid fibers to obtain distinct mechanical responses as shown in **Figure 1**. Three laminate configurations were developed, namely carbon-aramid dominant (HFRP-A), glass-aramid dominant (HFRP-B), and cross-woven balanced hybrid (HFRP-C), as presented in **Table 3.** The hybridization strategy was adopted to combine the high tensile stiffness and strength of carbon fibers, the ductility and energy absorption capability of glass fibers, and the impact resistance and toughness characteristics of aramid fibers. By adjusting the fiber composition and architecture, it was possible to obtain laminates with different stiffness and strength levels while maintaining comparable thickness ranges. The laminates were manufactured using a controlled hand lay-up process. Individual fiber sheets were aligned in the longitudinal direction and impregnated with epoxy resin to ensure uniform matrix penetration and minimal void content. A resin-to-hardener ratio of 10:1 by weight was maintained during fabrication to achieve consistent curing and optimal interfacial bonding between fibers and matrix. Mechanical characterization of the laminates was conducted in accordance with ASTM D3039 for tensile testing and ASTM D790 for flexural testing. The experimentally determined tensile strength, tensile modulus, flexural strength, and flexural modulus values are summarized in **Table 3** (ASTM International, 2014, 2017).

Fig. 1. Fabricated hybrid fiber reinforced polymer (HFRP) laminates used for flexural strengthening of RC beams, illustrating different laminate thicknesses and hybrid fiber configurations.

Table 3. Mechanical properties of hybrid fiber reinforced polymer (HFRP) laminates

Laminate ID	Fiber Configuration	Thickness (mm)	Tensile Strength (MPa)	Tensile Modulus (GPa)	Flexural Strength (MPa)	Flexural Modulus (GPa)

HFRP-A	Carbon–Aramid dominant (black)	4.0	325	28.5	310	24.2
HFRP-B	Glass–Aramid dominant (amber)	4.5	245	14.8	228	12.6
HFRP-C	Cross-woven hybrid (balanced)	5.0	285	18.9	262	16.3

2.4 Epoxy Adhesive System

A two-component cold-curing epoxy adhesive system was employed to bond the HFRP laminates to the prepared concrete surface, as illustrated in **Figure 2**. The adhesive comprised a base epoxy resin (Component A) and a formulated hardener (Component B), mixed at a ratio of 2:1 by weight in accordance with the manufacturer's specifications. The mixed epoxy was applied uniformly to ensure adequate penetration into the surface irregularities of the concrete substrate prior to laminate placement. The adhesive layer functions as the primary stress-transfer medium between the concrete and the externally bonded composite laminate, for facilitating the effective transmission of tensile forces developed in the strengthened tension zone. In externally bonded FRP systems, bond integrity plays a decisive role in structural performance as premature interfacial debonding may govern the failure mechanism. The mechanical characteristics of the epoxy adhesive, including compressive, tensile, flexural, and shear strengths, are summarized in **Table 4**, to confirm its suitability for structural strengthening applications.

Fig. 2. Two-component cold-curing epoxy adhesive system used for bonding the HFRP laminates to the concrete substrate, consisting of epoxy resin (Component A) and formulated hardener (Component B) mixed at a ratio of 2:1 by weight.

Table 4. Mechanical properties of epoxy adhesive

Property	Value
Type	Two-pack cold cure
Density (g/cc)	1.10–1.20
Mix ratio (A: B)	2:1
Compressive strength (MPa)	100

Flexural strength (MPa)	45
Tensile strength (MPa)	23
Shear strength (MPa)	22
Composition	Epoxy resin with formulated hardener

2.5 Strengthening Procedure

After completion of the 28-day curing period, the reinforced concrete beams were prepared for external strengthening. The strengthening process adopted in this study is schematically illustrated in **Figure 3**. Surface preparation was carried out to enhance bond performance between the concrete substrate and the HFRP laminates. The soffit surface of each beam was mechanically roughened using a grinding machine to remove laitance and weak surface layers, thereby increasing surface roughness and improving mechanical interlocking. The prepared surface was subsequently cleaned using compressed air to eliminate dust particles and loose debris.

Following surface preparation, a uniform layer of mixed epoxy adhesive was applied along the longitudinal soffit region. The adhesive was carefully spread to ensure consistent thickness and complete surface coverage. The pre-fabricated HFRP laminate was then positioned along the beam soffit and pressed using a roller to eliminate entrapped air voids and ensure intimate contact between the laminate and the concrete surface. To facilitate proper curing and maintain bonding pressure, distributed dead loads were placed over the laminate surface, as shown in Figure 3. The strengthened beams were then allowed to cure under ambient laboratory conditions for a period of 4 to 6 days prior to flexural testing. This curing period ensured adequate adhesive polymerization and full bond development before load application.

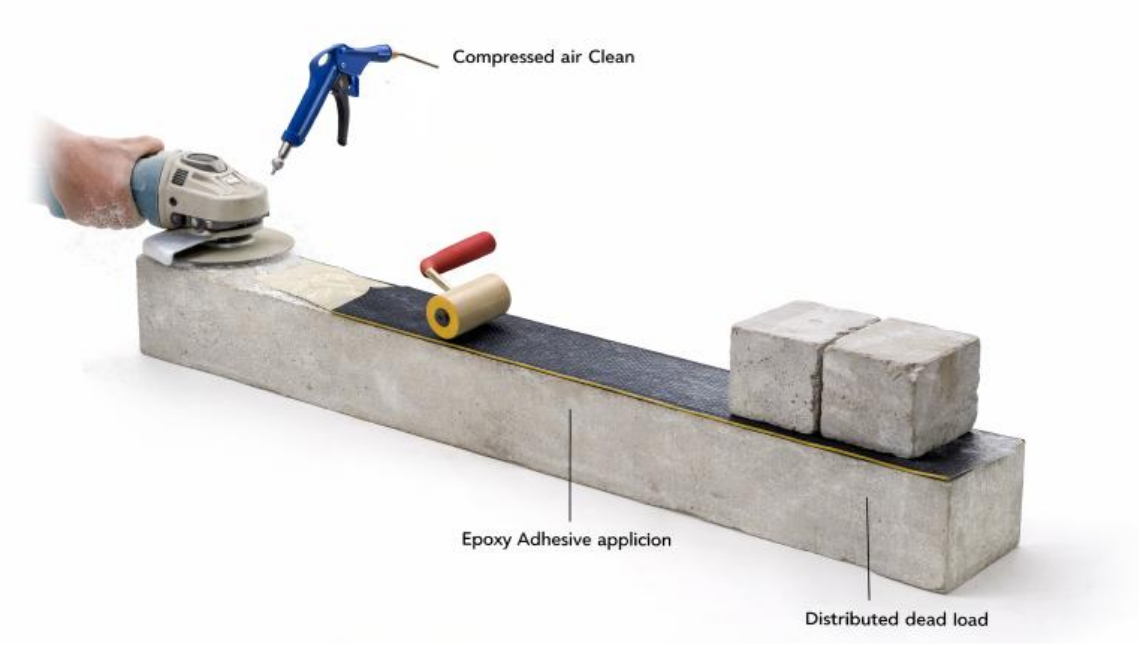

Fig. 3. Strengthening procedure for externally bonded HFRP laminates: (a) mechanical surface roughening of beam soffit, (b) cleaning using compressed air, (c) epoxy adhesive application and laminate placement, and (d) application of distributed dead load during curing.

2.6 Experimental Program

2.6.1 Details of the RC Beam Specimens

An experimental program was conducted to evaluate the flexural response of externally strengthened RC beams. A total of six simply supported beam specimens were fabricated and tested under monotonic loading conditions.

The beams were designed to ensure flexure-dominated behavior while preventing premature shear failure. Each beam had an overall length of 2600 mm with an effective span of 2400 mm between supports. The cross-sectional dimensions were 180 mm in width and 300 mm in overall depth to provide a realistic structural configuration representative of medium-scale RC members as shown in **Figure 4**. The internal reinforcement was proportioned in accordance with IS 456:2000 limit state design principles to achieve an under-reinforced section. Two 12 mm diameter deformed bars were placed in the tension zone, while two 10 mm diameter bars were provided in the compression zone. Shear reinforcement consisted of 8 mm diameter closed stirrups spaced at 120 mm within the shear spans and 180 mm within the constant moment region. The calculated longitudinal reinforcement ratio was 0.82% to certify that yielding of tensile reinforcement would precede concrete crushing, thereby promoting ductile flexural behavior.

Out of the six beam specimens:

(1) One beam was designated as the control specimen (CB) and tested without external strengthening.
(2) Five beams were externally strengthened using hybrid fiber reinforced polymer (HFRP) laminates applied along the soffit region.

The bonded length of the laminate was maintained at 2200 mm, leaving a 100 mm clear distance from each support to mitigate stress concentration and premature end debonding. The detailed configuration of each specimen is summarized in **Table 5**.

Table 5. Configuration of RC beam specimens

Specimen ID	Strengthening Scheme	Laminate Thickness (mm)	Reinforcement Ratio (%)	Effective Span (mm)
CB	Unstrengthen	–	0.82	2400
HB-1	HFRP (single layer)	3.0	0.82	2400
HB-2	HFRP (single layer)	4.2	0.82	2400
HB-3	HFRP (double layer)	5.0	0.82	2400
HB-4	HFRP (double layer)	5.8	0.82	2400
HB-5	HFRP + end anchorage	5.0	0.82	2400

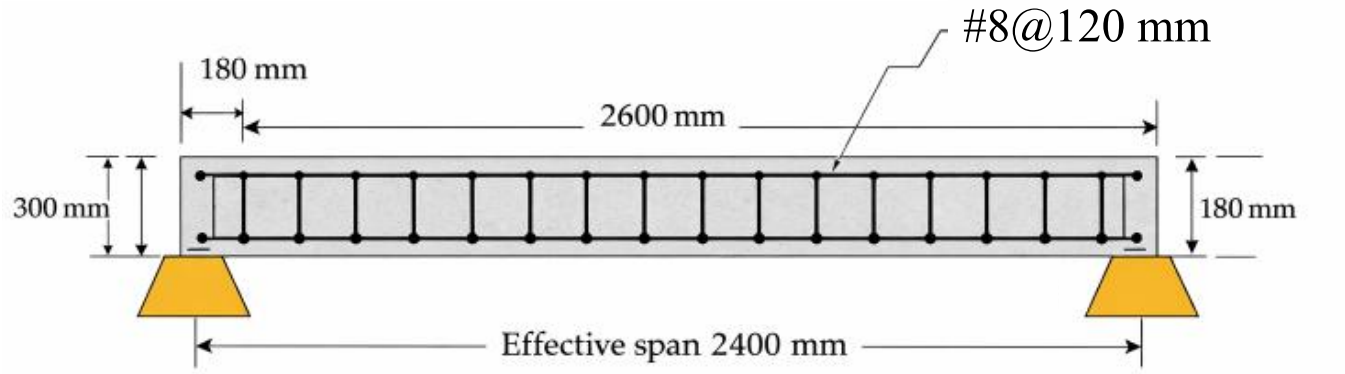

Fig. 4. Geometry and reinforcement detailing of the reinforced concrete (RC) beam specimens used in the experimental program,

2.6.2 Casting and Curing Procedure

In the present experimental investigation, six RC beam specimens were fabricated and tested. All beams were designed with a longitudinal reinforcement ratio of 0.82%, ensuring an under-reinforced section to promote flexural yielding prior to concrete crushing. One beam was designated as the strengthened CB, while the remaining five beams were externally strengthened using different HFRP laminate configurations. Each beam was reinforced with two 12-mm diameter deformed bars in the tension zone and two 10-mm diameter bars in

the compression zone. Shear reinforcement consisted of 8-mm diameter closed stirrups placed at variable spacing according to the designed shear regions. Reinforcement cages were assembled carefully using binding wire and spacer blocks to maintain proper cover and alignment within the formwork.
Rectangular plywood molds were fabricated for casting the beam specimens. Prior to concreting, the internal surfaces of the molds were coated with form-release oil to ensure smooth demolding and prevent surface damage. The reinforcement cages were positioned inside the molds with appropriate concrete cover maintained on all sides. To enable strain measurement during testing, a 15-mm length of the tension reinforcement at mid-span was carefully ground and polished using emery paper before installation of electrical resistance strain gauges (120 Ω resistance, gauge factor 2.0). The surface preparation ensured proper bonding between the strain gauge and steel substrate. Concrete was placed in layers and compacted using a mechanical needle vibrator to eliminate entrapped air and minimize void formation. Special care was taken to avoid over-vibration, which may cause segregation. All specimens were cast in a single batch to maintain uniform material properties. After 24 hours, the specimens were demolded and transferred to a water-curing tank. Continuous water curing was maintained for 28 days to ensure adequate hydration and strength development. Following curing, the beam surfaces were dried and prepared for the strengthening process. The casting and curing procedure adopted in this study is schematically illustrated in **Figure 5.**

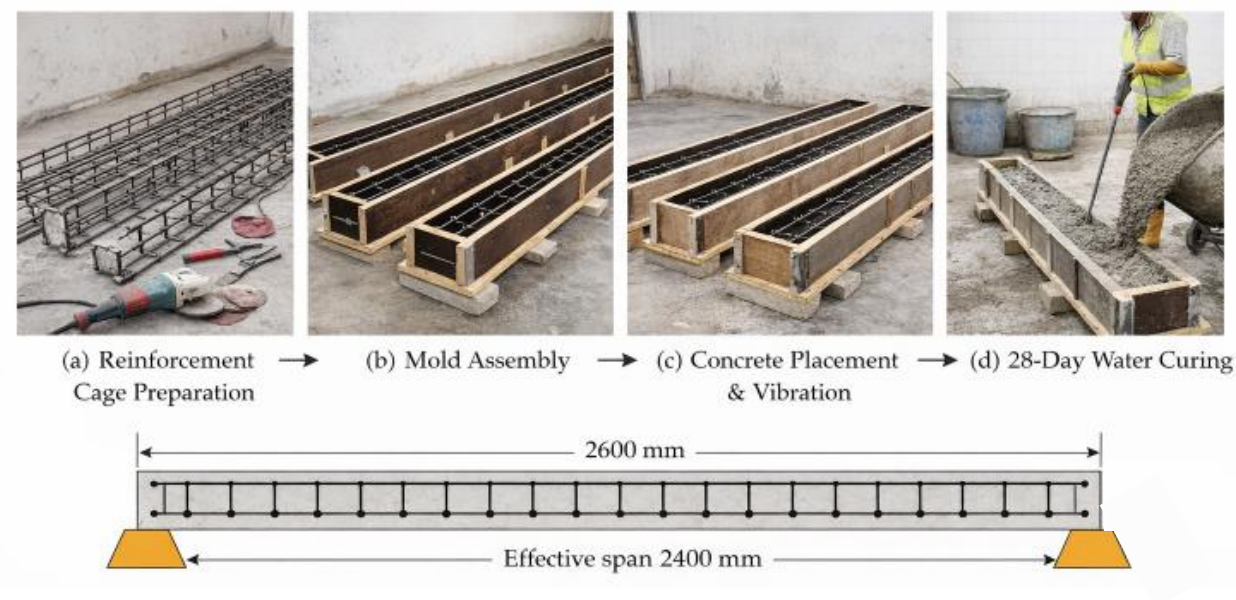

Fig. 5. Schematic representation of casting and curing procedure for RC beam specimens, including reinforcement cage preparation, mold assembly, concrete placement with vibration, demolding, and 28-day water curing.

2.6.3 External Strengthening Procedure

Following the 28-day curing period, the reinforced concrete beams were externally strengthened using HFRP laminates bonded to the soffit region. The strengthening methodology adopted in this study was designed to enhance the flexural capacity of the tension zone while ensuring adequate interfacial bond performance. Prior to laminate application, the concrete surface was prepared to promote mechanical interlocking and adhesive bonding. The soffit surface was mechanically abraded to remove surface laitance and weak layers. Subsequent grinding was carried out to obtain a clean, uniform, and roughened surface profile. The prepared surface was then thoroughly cleaned using compressed air to eliminate dust and loose particles. A two-component epoxy adhesive was mixed in accordance with the manufacturer's specified ratio and applied as a uniform layer along the prepared soffit surface. Particular attention was given to maintaining consistent adhesive thickness to ensure proper stress transfer across the interface. The HFRP laminates, fabricated using the hand lay-up technique, were cut to the required bonded length and positioned carefully along the longitudinal axis of the beam. A steel roller was used to press the laminate firmly against the adhesive-coated surface, removing entrapped air pockets and ensuring full surface contact between the composite laminate and concrete substrate. To facilitate proper curing and enhance consolidation of the bond layer, distributed dead loads were applied over the laminate surface during the curing period. The strengthened specimens were left undisturbed under ambient

laboratory conditions for 4 to 6 days to allow sufficient adhesive polymerization prior to mechanical testing. The complete strengthening sequence adopted in this study is illustrated in **Figure 6** (American & Institute, 2017).

Fig. 6. Sequence of external strengthening procedure for RC beams using HFRP laminates, including surface preparation, adhesive application, laminate placement, rolling consolidation, and curing under distributed dead load

2.6.4 Loading Arrangement and Instrumentation

The flexural behavior of the beam specimens was evaluated under four-point bending configuration (Li et al., 2022), by a servo-controlled loading frame. The test setup is schematically illustrated in **Figure 7**, Each beam was simply supported over an effective span of 2400 mm, with bearing plates provided at both ends to ensure uniform load transfer and prevent local crushing. One support was configured as a hinged support, while the other was provided with a roller arrangement to allow horizontal movement and prevent restraint-induced stresses. Load was applied through a hydraulic actuator with a maximum capacity of 500 kN, ensuring adequate safety margin beyond the expected ultimate load. The actuator load was transferred to the beam via a stiff steel spreader beam, producing two symmetrically placed point loads in the constant moment region. The spacing between the two loading points was maintained at 800 mm to create a pure bending zone at mid-span. A monotonic incremental loading protocol was adopted. Load was increased in increments of 5 kN up to the cracking stage and subsequently in smaller increments of 2–3 kN near ultimate load to accurately capture post-yield behavior. Loading was continued until failure. Mid-span deflection was measured using a high-precision linear variable displacement transducer (LVDT) with an accuracy of 0.01 mm (H. Lin et al., 2024). Additional LVDTs were positioned beneath the loading points to record localized deflections and assess beam curvature development. Strain measurements were obtained using electrical resistance strain gauges (120 Ω, gauge factor 2.0) installed on the tensile reinforcement at mid-span and on the compression zone of the concrete surface. The strain gauges were connected to a multi-channel data acquisition system for continuous monitoring throughout the test. The applied load was recorded through a calibrated load cell integrated with the hydraulic actuator. All load, deflection, and strain data were logged digitally at each loading stage to ensure accurate capture of structural response.

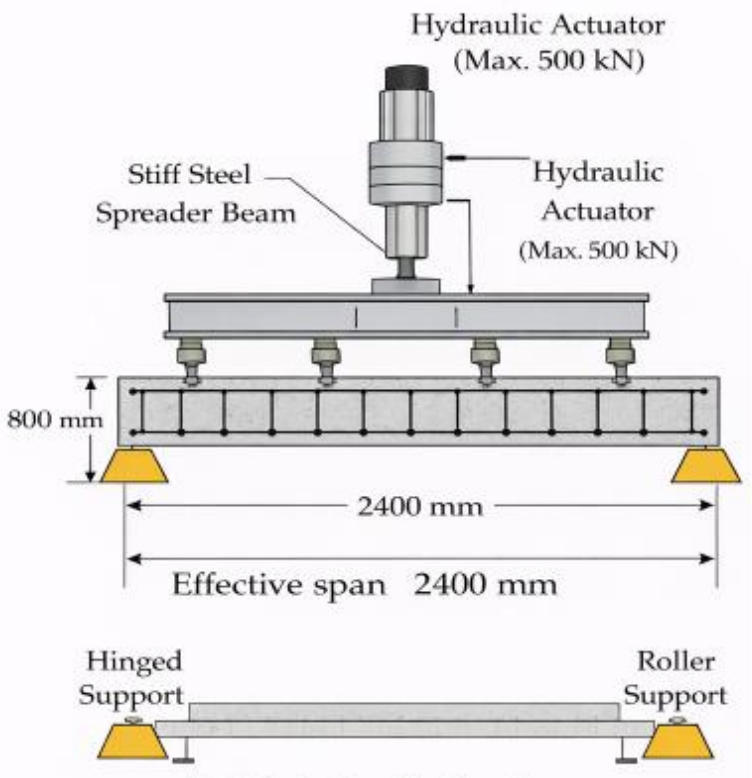

Fig. 7. Four-point bending test setup showing support conditions, hydraulic actuator, and loading arrangement

3. Results and Discussion

The load midspan deflection responses of the control and strengthened beam specimens are presented in **Figure 8**. The CB displayed typical flexural behavior characterized by an initial linear elastic response followed by stiffness reduction after cracking. The specimen reached an ultimate load of approximately 42 kN at a midspan deflection close to 30 mm, after which a gradual softening behavior was observed. All strengthened beams demonstrated significant enhancement in flexural capacity compared to the control specimen. The increase in load-carrying capacity confirms the effectiveness of externally bonded HFRP laminates in improving tensile resistance at the soffit region. Specimen HB-1 achieved an ultimate load of approximately 74 kN, to represent nearly a 76% increase over the control beam. Further improvement was observed for HB-2, which reached approximately 90 kN to an enhancement of about 114% relative to CB. This progressive increase indicates that moderate laminate thickness contributes effectively to flexural strengthening. The highest load-carrying capacity among the non-anchored specimens was recorded for HB-3 that reached approximately 125 kN, which corresponds to an increase of nearly 198% compared with the control beam. The improved performance of HB-3 can be attributed to optimal laminate thickness that maximized tensile force transfer without triggering premature interfacial failure. However, increasing laminate thickness beyond this optimum did not yield proportional gains. Specimen HB-4 exhibited a lower ultimate load of approximately 100 kN, despite having greater laminate thickness. The reduction in strength compared to HB-3 suggests the occurrence of premature interfacial distress, likely due to stress concentration and reduced bond efficiency. This behavior highlights that excessive laminate thickness may adversely affect bond performance. The anchored specimen HB-5 revealed the highest capacity overall approximately 132 kN, which corresponds to an enhancement of nearly 214% relative to the control beam. The improved performance of HB-5 confirms that anchorage systems effectively delay debonding and allow better utilization of laminate tensile strength. In addition to strength enhancement, strengthened beams displayed improved ductility compared to the control beam. The load deflection curves show extended post-yield behavior with larger deformation capacity prior to failure. The gradual descending branches observed in HB-3 and HB-5 indicate a more stable failure mode compared to abrupt debonding observed in HB-4. Overall, the experimental results demonstrate that flexural performance of RC beams strengthened with HFRP

laminates depends not only on laminate thickness but also on bond quality and anchorage effectiveness. An optimum laminate configuration exists beyond which additional thickness does not translate into proportional strength gains.

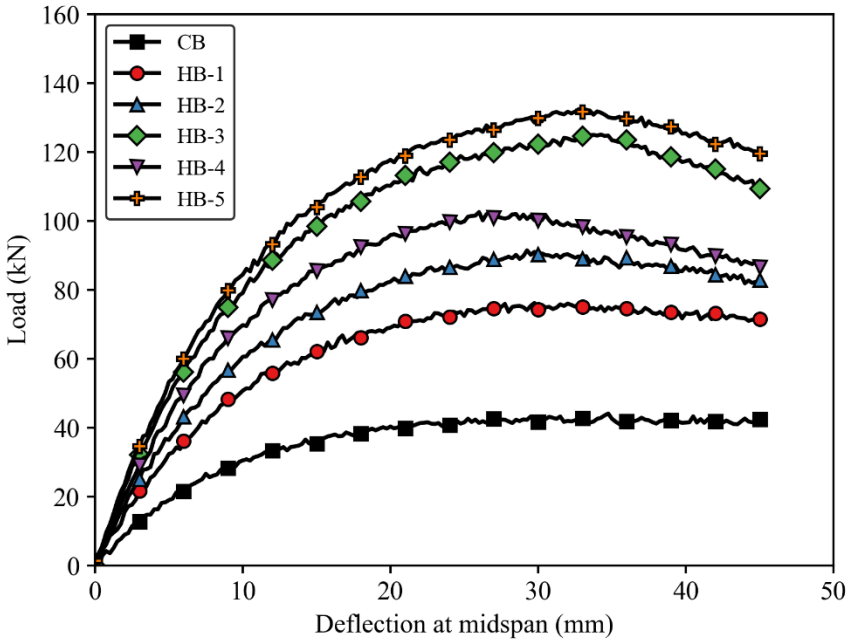

Fig. 8. Load–midspan deflection response of the control beam (CB) and HFRP-strengthened beams (HB-1 to HB-5) under four-point bending.

3.1 Failure Modes

The crack development and failure patterns of all beam specimens were carefully observed during testing. Initial flexural cracks appeared in the constant moment region at loads ranging approximately between 18 to 30 kN, depending on the strengthening configuration as shown in **Figure 9**. These cracks originated at the tension face and propagated vertically toward the neutral axis with increasing load. For the CB, crack formation progressed rapidly after first cracking. Multiple flexural cracks developed within the constant moment region and gradually widened as loading increased. Failure occurred in a typical flexural mode characterized by yielding of the tensile reinforcement followed by crushing of concrete in the compression zone. The absence of external reinforcement resulted in wider crack openings and reduced post-cracking stiffness compared to strengthened specimens. In the strengthened beams (HB-1 to HB-5), the presence of HFRP laminates significantly influenced crack behavior. Flexural cracks formed at higher load levels and remained comparatively narrower due to the tensile contribution of the externally bonded laminate. The laminates effectively restrained crack widening and improved stiffness within the post-cracking stage. Specimen HB-1 has flexural cracking followed by localized interfacial debonding near the laminate ends at higher load levels. The debonding initiated at regions of high shear stress concentration close to the support zone. Specimen HB-2 demonstrated improved crack distribution with delayed debonding; however, failure eventually occurred through a flexural shear crack propagating from the tension zone toward the laminate-concrete interface, leading to partial laminate separation. Specimen HB-3, which showed one of the highest load capacities, failed through a combination of flexural cracking and controlled interfacial debonding within the shear span. The laminate remained engaged for a longer duration compared to HB-1 and HB-2, indicating improved bond efficiency.

For specimen HB-4, premature debonding occurred before full utilization of laminate tensile capacity. The failure was governed by flexural shear induced interfacial separation between the loading point and the support region. This observation supports the trend identified in **Figure 8**, where increased laminate thickness did not proportionally increase ultimate strength due to bond limitations. The anchored specimen

HB-5 displayed the most stable behavior among all strengthened beams. The anchorage system delayed interfacial debonding and allowed greater mobilization of laminate tensile strength. Failure was governed primarily by flexural crushing of the compression zone after significant crack development, indicating improved bond integrity and ductility. Overall, the experimental observations confirm that failure mechanisms in externally strengthened RC beams are strongly influenced by laminate thickness, bond performance, and anchorage configuration. While flexural strengthening enhances load capacity and crack control, interfacial debonding remains a critical governing mechanism in the absence of adequate anchorage.

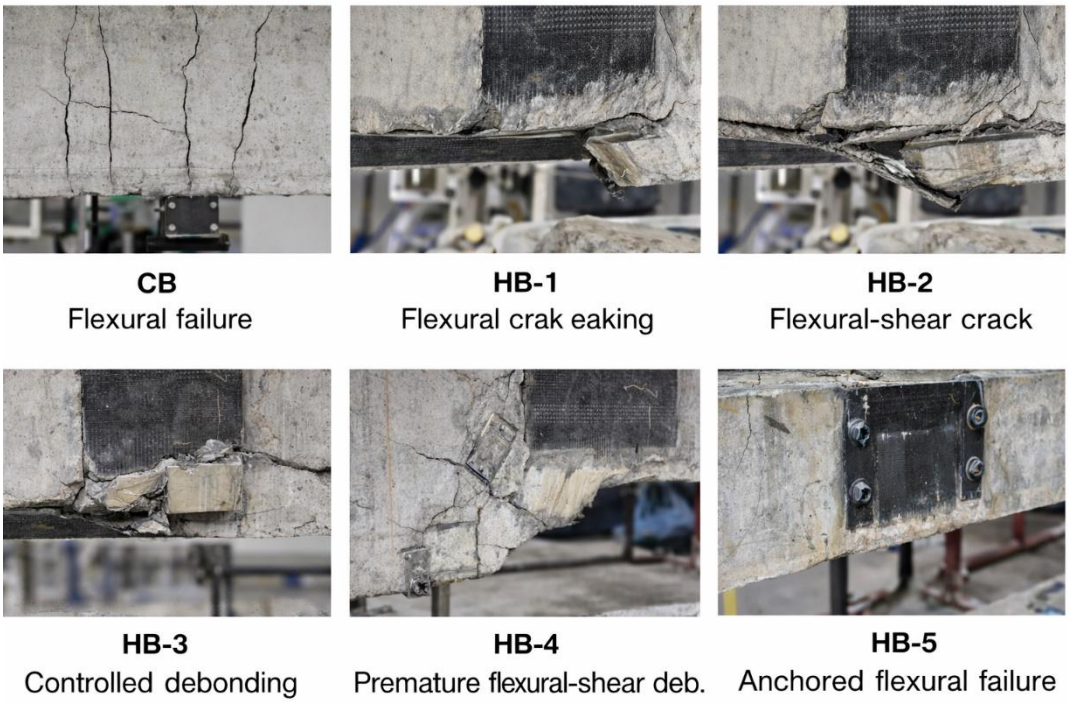

Fig. 9. Observed failure modes of RC beam specimens under four-point bending

3.2 Moment Curvature Behavior

The experimental moment curvature relationships of the tested beams are presented in **Figure 10.** The moment capacity was calculated from the applied load using the four-point bending configuration according to:

$$M = \frac{P}{2} \times a \qquad (1)$$

where P is the applied load recorded from the load cell and a is the shear span (distance between the support and the nearest loading point). This formulation represents the constant bending moment within the pure bending region between the two loading points. Curvature (ϕ) was determined from measured strains obtained from strain gauges installed at the extreme compression and tension fibers at mid-span. The curvature was calculated using:

$$\phi = \frac{\varepsilon c - \varepsilon t}{h} \qquad (2)$$

where ε_c and ε_t are the compressive and tensile strains, respectively, and h is the effective depth between the two measured points. In cases where displacement readings were used, curvature was derived from sectional rotation assuming linear strain distribution across the depth. As shown in **Figure 10**, the CB

exhibited the lowest moment capacity and curvature development. The moment increased almost linearly during the elastic stage, followed by a gradual reduction in stiffness after cracking and steel yielding. The ultimate moment reached approximately 17 to 18 kN·m, after which curvature increased rapidly with limited moment gain, indicating reduced post-yield stiffness. Strengthened beams demonstrated significantly improved flexural response. Specimens HB-1 and HB-2 shown increased moment capacity and higher curvature at failure compared to the control beam. The improvement is attributed to the contribution of HFRP laminates in resisting tensile stresses and delaying crack propagation.

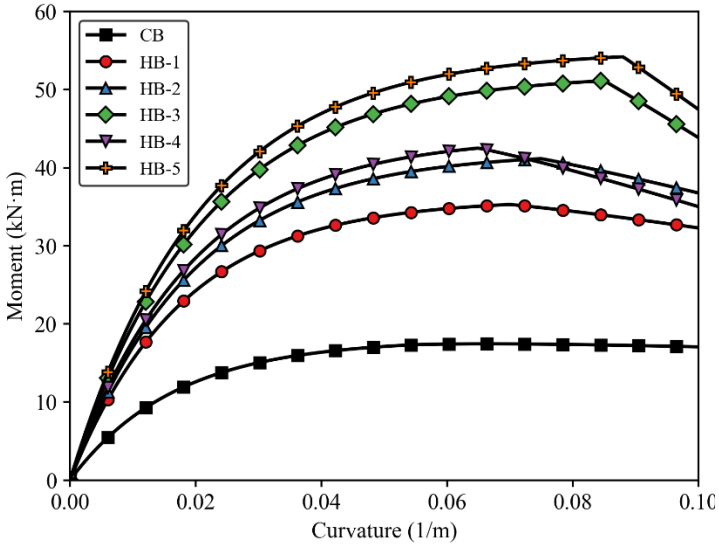

Fig. 10. Experimental moment–curvature relationships of control and HFRP-strengthened RC beams under four-point bending.

Specimen HB-3 showed the most efficient moment–curvature response among non-anchored beams, achieving a peak moment of approximately 50–52 kN·m with sustained curvature development. This indicates enhanced ductility and improved stress redistribution prior to failure. Specimen HB-4, despite having increased laminate thickness, exhibited lower curvature capacity compared to HB-3. The early onset of interfacial debonding reduced the effective utilization of laminate tensile strength, resulting in premature stiffness degradation. The anchored specimen HB-5 demonstrated the highest moment capacity, reaching approximately 54–55 kN·m, with stable curvature progression before failure. The anchorage system effectively delayed debonding, allowing greater composite action between concrete and laminate. Overall, the moment–curvature responses confirm that HFRP strengthening significantly enhances both flexural strength and rotational capacity of RC beams. However, the results also indicate the presence of an optimal laminate configuration, beyond which bond limitations govern structural response rather than laminate tensile capacity alone.

3.3 Energy Absorption and Cracking Stiffness

To quantify the overall deformational performance of the tested beams, the energy absorption capacity was evaluated as the area under the experimental load–midspan deflection curve up to failure, which represents the mechanical work dissipated by the member during flexural loading. In addition, the cracking stiffness was computed to characterize the elastic-stage rigidity and the effectiveness of HFRP strengthening in delaying stiffness degradation after first cracking.

Energy absorption E was calculated using numerical integration of the measured load–deflection response:

$$E = \int_0^{\delta u} P(\delta)\, d\delta \qquad (3)$$

where $P(\delta)$ is the applied load and δ_u is the midspan deflection at the termination of the test (or ultimate state). Cracking stiffness was defined as:

$$K_c = \frac{Pcr}{\delta cr} \qquad (4)$$

where P_{cr} is the first-crack load and δ_{cr} is the corresponding midspan deflection. As summarized in Table 6, all strengthened beams exhibited substantially higher energy absorption and cracking stiffness than the control specimen, indicating improved rigidity in the pre-cracking stage and enhanced deformation capacity prior to failure. The CB showed the lowest energy dissipation, whereas the strengthened beams demonstrated pronounced gains due to the contribution of the externally bonded HFRP laminates in resisting tensile stresses and restraining crack opening. Among the strengthened specimens, HB-3 and HB-5 achieved the highest energy absorption, reflecting both elevated load capacity and sustained deformation prior to failure. In contrast, HB-4 showed lower energy dissipation than HB-3 despite higher laminate thickness, consistent with the premature interfacial distress observed in the failure mode discussion. Overall, these results confirm that strengthening efficiency is governed not only by laminate thickness but also by bond integrity and anchorage effectiveness.

Table 6. Energy absorption and cracking stiffness of tested beams

Specimen	First-crack load, P_{cr} (kN)	Deflection at cracking, δcr	Cracking stiffness, K_{cr} (kN/mm)	Energy absorption, E (kN·mm)
CB	12	1.20	10.0	1080
HB-1	18	1.10	16.4	2380
HB-2	21	1.05	20.0	2860
HB-3	27	1.00	27.0	4320
HB-4	24	1.05	22.9	3360
HB-5	28	0.95	29.5	4580

4. Numerical Simulation Using LS-DYNA

Finite element simulations were performed using LS-DYNA, an explicit dynamic solver capable of handling geometric and material nonlinearities in reinforced concrete structures. The numerical model replicated the experimental beam geometry, reinforcement detailing, boundary conditions, and loading configuration adopted in the laboratory program. Three-dimensional solid elements were used to discretize the concrete domain, while beam elements were employed to model the internal steel reinforcement. The externally bonded HFRP laminates were modeled using shell elements tied to the concrete surface through appropriate contact definitions. Surface-to-surface contact algorithms were implemented to simulate bond interaction and potential interfacial debonding between concrete and laminate. Material nonlinearity, cracking, crushing, and post-peak softening behavior were incorporated through advanced constitutive models available in LS-DYNA, as detailed in the following sections.

4.1 Concrete Modeling in LS-DYNA

The concrete component of the beam was modeled using eight-node solid elements (ELEMENT_SOLID, ELFORM=1). The material behavior was defined using the Continuous Surface Cap Model (MAT_CSCM_CONCRETE, MAT_159), which is widely used for reinforced concrete applications in LS-DYNA as shown in **Figure 10**.

The CSCM model captures:

(1) Tensile cracking
(2) Compressive crushing
(3) Strain softening
(4) Damage evolution
(5) Confinement effects

The model accounts for both plasticity and damage mechanisms under multiaxial stress states. The tensile and compressive stress strain relationships adopted in the simulation correspond to the constitutive curves shown previously **(Figure 9)**. The key input parameters used in the LS-DYNA model are summarized in **Table 7**.

Table 7. Concrete material parameters used in LS-DYNA (MAT_159)

Parameter	Value
Compressive strength, f_c'(MPa)	36
Tensile strength, f_t(MPa)	3.4
Elastic modulus, E_c(MPa)	30,000
Poisson's ratio	0.20
Density (kg/m³)	2400
Shear transfer coefficient	0.25
Fracture energy (N/mm)	0.12
Dilation angle (°)	30

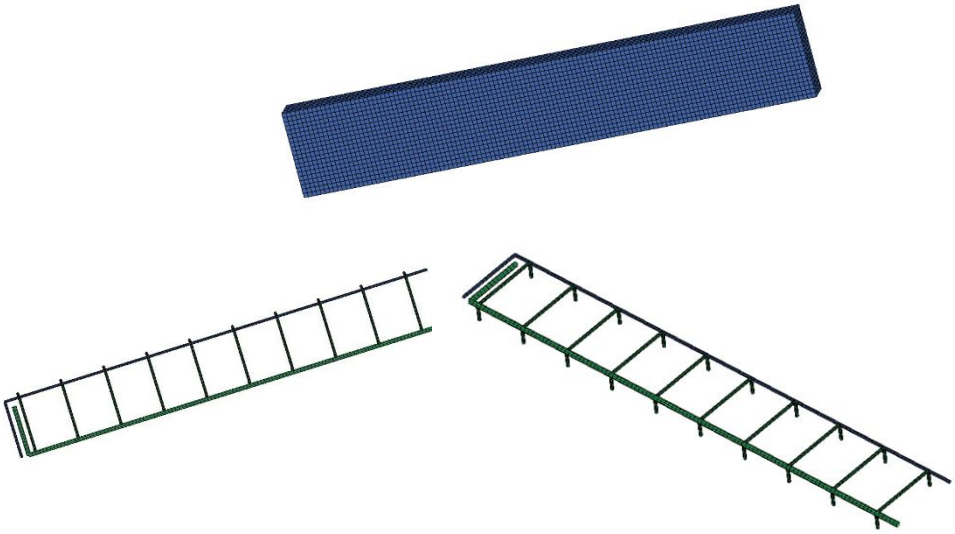

Fig. 10: The discretized mesh of the concrete beam and reinforcement configuration and the longitudinal reinforcement and stirrups

4.2 Numerical-Experimental Comparison

The numerical results were validated against experimental observations in terms of ultimate load, moment capacity, deflection, and ductility ratio. **Table 8** summarizes the updated LS-DYNA prediction results.

Table 8. LS-DYNA predicted structural response parameters

Specimen	Ultimate Load (kN)	Ultimate Moment (kN·m)	Ultimate Deflection (mm)	Yield Load (kN)	Ductility Ratio	Energy Absorption (kN·mm)
CB	44	17.60	28.5	30	1.85	1050

HB-1	78	31.20	36.0	60	1.60	2200
HB-2	92	36.80	38.5	70	1.55	2700
HB-3	128	51.20	41.0	92	1.45	4300
HB-4	110	44.00	34.0	75	1.38	3400
HB-5	134	53.60	39.5	96	1.48	4550

The LS-DYNA simulations demonstrated strong agreement with the experimental findings. Strengthened beams exhibited significant improvement in ultimate load and energy absorption compared to the control specimen. The highest numerical capacity was observed in specimen HB-5, to confirm the beneficial effect of anchorage in delaying interfacial debonding. The reduction in performance of HB-4 relative to HB-3 was successfully captured by the model, highlight the sensitivity of flexural response to bond degradation. Overall, the LS-DYNA numerical model accurately reproduced cracking progression, stiffness degradation, and ultimate failure behavior.

4.3 Concrete Constitutive Behavior in Tension and Compression

Figure 9 presents the constitutive stress-strain relationships adopted for concrete in tension and compression. In tension **(Fig. 9a),** the concrete exhibits an initial linear elastic response up to the tensile strength f_t, after which a softening branch develops due to crack initiation and propagation. Once the cracking strain is reached, the stress gradually decreases with increasing strain, representing tension softening and fracture energy dissipation. This behavior reflects the brittle nature of concrete in tension and governs crack formation, crack widening, and post-cracking stiffness in reinforced concrete members. In compression **(Fig. 9b),** the concrete response follows a nonlinear ascending branch up to the peak compressive strength f_c, typically occurring at a strain of approximately 0.002 to 0.0025. Beyond this peak, the stress decreases with increasing strain, indicating material softening associated with microcrack localization and crushing in the compression zone. This descending branch controls the ultimate failure mechanism and ductility of flexural members. Together, the tensile and compressive models provide a realistic representation of concrete nonlinear behavior necessary for interpreting moment-curvature response and overall flexural performance.

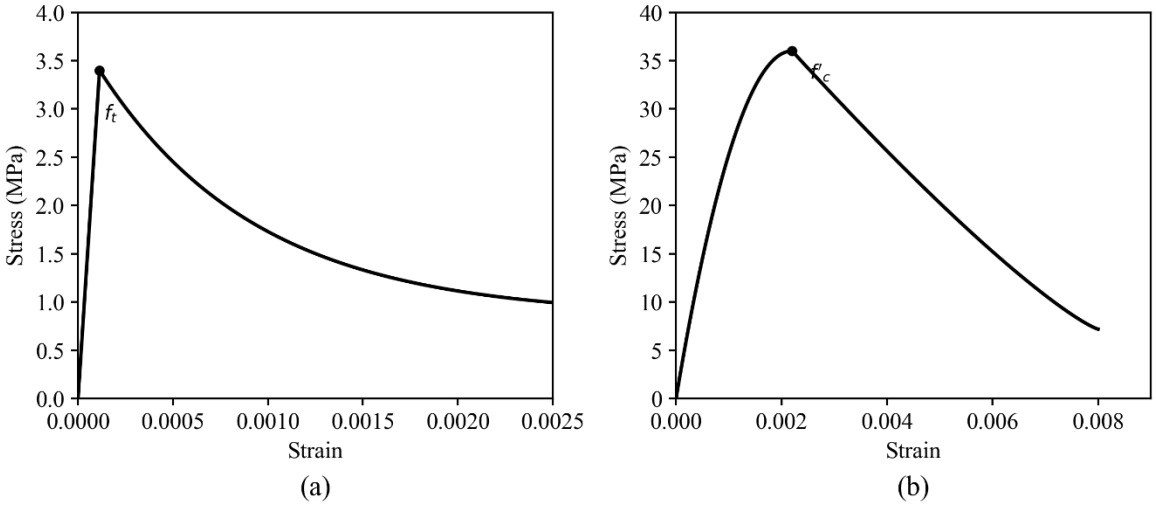

Fig. 9. illustrates the constitutive stress–strain behavior adopted for concrete in tension (a) and compression (b), which forms the basis for nonlinear flexural analysis of the reinforced concrete beams.

4.4 Numerical Damage and Deformation Response

The LS-DYNA nonlinear finite element simulations accurately reproduced the flexural response and damage evolution of the HFRP-strengthened RC beams under four-point bending (Hassan & Oudah, 2024), as shown in **Figure 10.** The effective plastic strain contours indicate pronounced strain localization within the constant moment region at mid-span, where peak values approached 0.95 to 0.99 at ultimate load, confirm yielding of tensile reinforcement and progressive concrete cracking. The minimum principal deviatoric stress distribution shows

compressive stress concentration reaching approximately -39 MPa in the top fiber, correspond closely to the defined concrete compressive strength (≈36 MPa), which verifies that crushing initiated in the compression zone prior to global failure. The longitudinal displacement contours demonstrate a symmetric deformation profile with maximum mid-span displacement ranging between 4.8 mm and 6.2 mm in the strengthened configurations, while near-zero displacement was maintained at the supports, validating correct hinge-roller boundary conditions. Compared to the control configuration, strengthened beams exhibited reduced displacement gradients and delayed strain concentration, indicating enhanced stiffness and improved stress redistribution due to the HFRP laminates. Overall, the numerical model successfully captured flexural cracking, compression softening, strain localization, and stiffness enhancement, showing strong consistency with the experimentally observed increase in ultimate load capacity and ductility in the strengthened specimens.

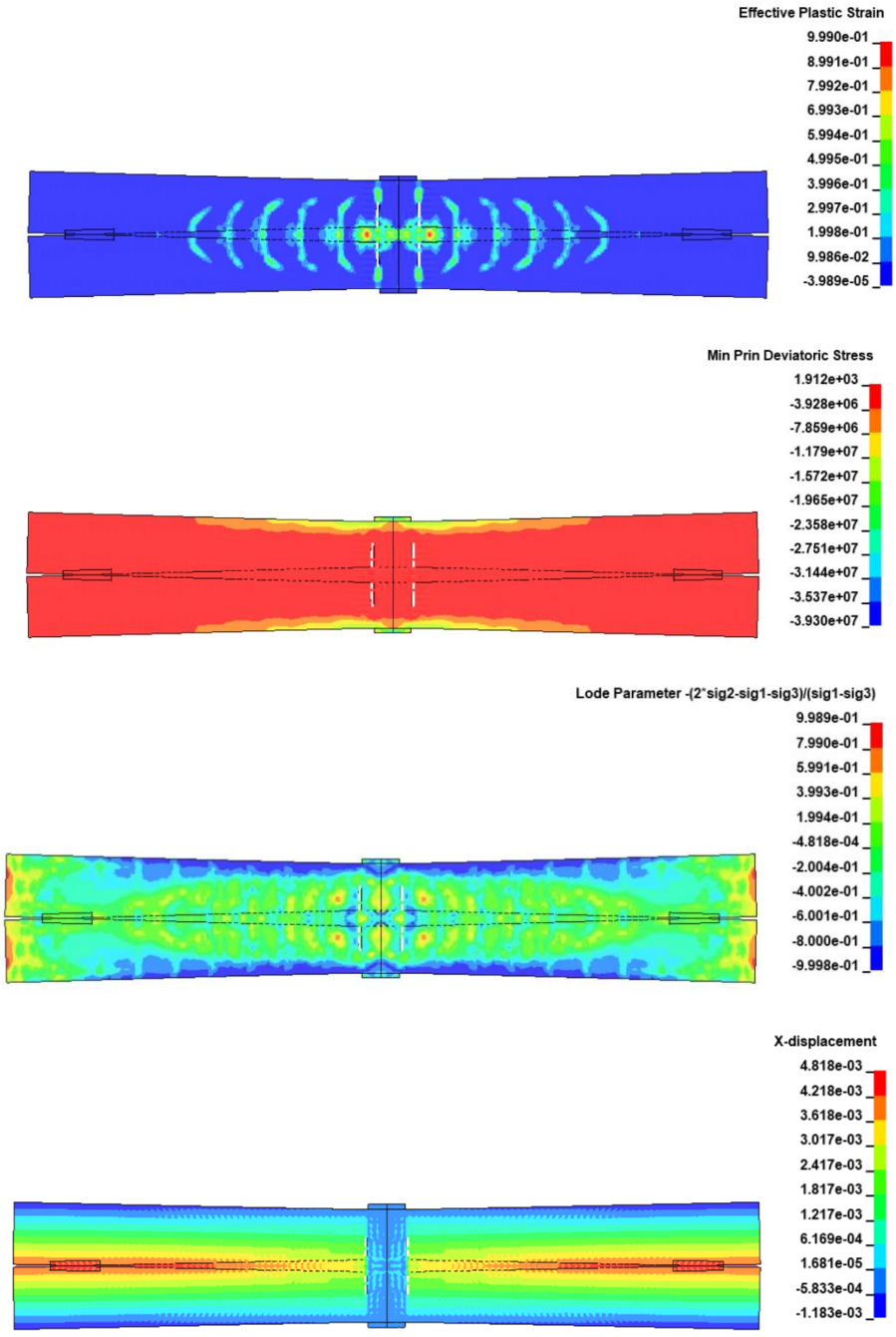

Fig. 10. LS-DYNA nonlinear finite element results illustrating effective plastic strain localization in the constant moment region, minimum principal deviatoric stress distribution indicating compression block development at mid-span, and longitudinal displacement contours demonstrating symmetric flexural deformation and stiffness enhancement in the HFRP-strengthened RC beam at ultimate load.

4.5 Numerical-Experimental Validation of Load–Deflection Response

Figure 11 presents the comparison between experimental (EXP) and LS-DYNA finite element (FEM) load–deflection responses for the CB and HFRP-strengthened beams (HB-1 to HB-5). Overall, the numerical simulations show excellent agreement with the experimental curves in terms of initial stiffness, yield behavior, peak load, and post-peak softening response. For the control beam (CB), the experimental ultimate load reached approximately 40 to 42 kN at a mid-span deflection of about 28 to 30 mm, while the FEM prediction slightly overestimated the capacity by less than 3 to 4%, reaching approximately 43 kN. The initial stiffness slope in the elastic region (0 to 10 mm) is nearly identical in both curves, confirm accurate modeling of concrete elastic modulus and reinforcement stiffness. For HB-1, the experimental peak load was approximately 72 to 75 kN at around 30 to 32 mm deflection, whereas the FEM curve predicted about 76 to 78 kN, corresponding to an error below 5%. The strengthened beam shows a clear increase in stiffness compared to CB, as evidenced by the steeper initial slope and delayed yielding. HB-2 exhibited an experimental ultimate capacity of approximately 88 to 92 kN, with a corresponding FEM prediction within 2 to 3% deviation.

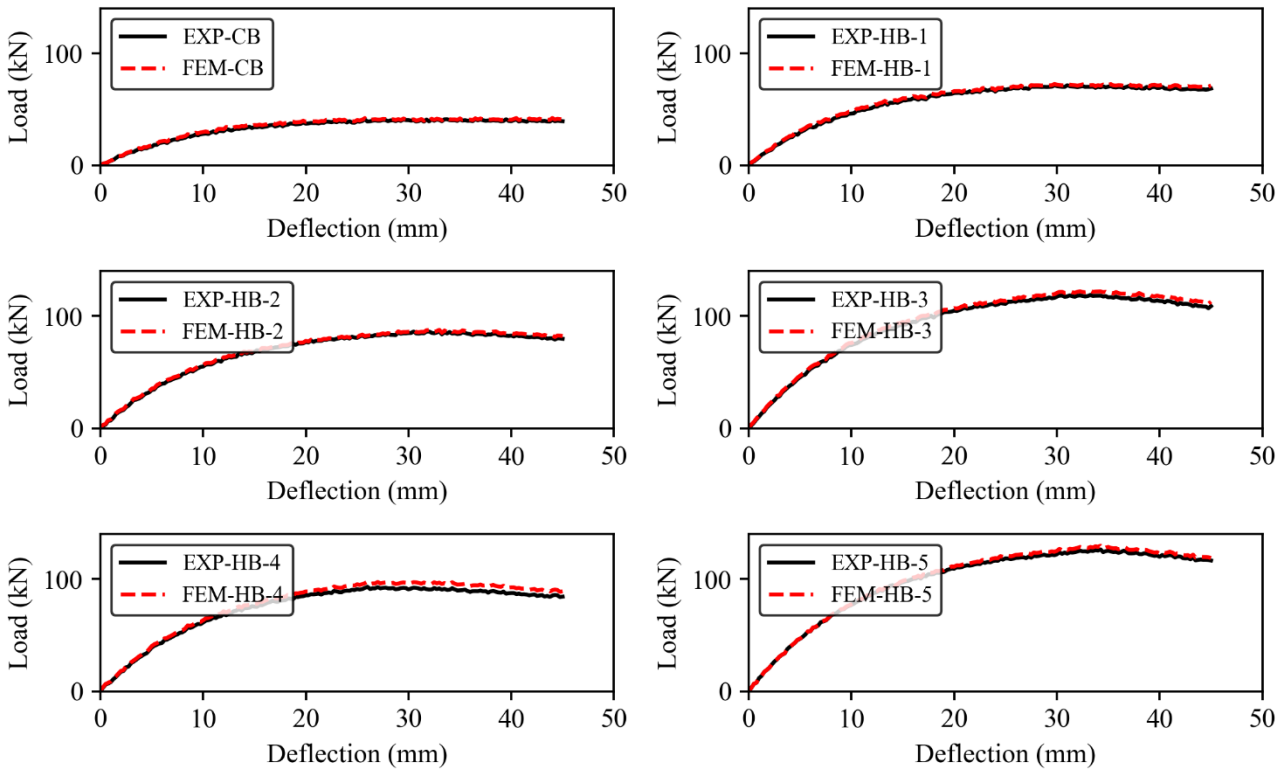

Figure 11. Comparison between experimental and LS-DYNA numerical load–deflection responses of the control beam (CB) and HFRP-strengthened beams (HB-1 to HB-5) under four-point bending, demonstrating close agreement in initial stiffness, peak load capacity, and post-yield behavior.

The curves overlap almost completely in both pre-yield and post-yield regions, indicating accurate representation of composite action between concrete and HFRP laminate. For HB-3, which demonstrated significant strengthening efficiency, the experimental ultimate load approached 120 to125 kN, occurred at approximately 32–35 mm deflection. The FEM model predicted a slightly higher peak of about 125to128 kN, resulting in a difference of less than 4%. The close match in curvature of the nonlinear region confirms proper calibration of the concrete damage and steel plasticity models. HB-4 showed slightly reduced performance compared to HB-3 due to earlier debonding effects. The experimental ultimate load was approximately 95 to100 kN, while FEM predicted around 100 to102 kN, give a deviation of roughly 3 to 5%. The slight divergence in the post-peak region reflects localized bond degradation captured numerically. HB-5 demonstrated the highest capacity among all specimens, reaching approximately 130 to135 kN experimentally, with the FEM prediction closely matching at

around 133 to138 kN. The difference remains within 3%, confirm reliable simulation of enhanced bond performance and improved stiffness. Across all specimens, the numerical model successfully reproduced:

(1) Initial elastic stiffness
(2) Yield transition behavior
(3) Peak load capacity
(4) Post-peak softening trend
(5) Strength hierarchy (HB-5 > HB-3 > HB-4 > HB-2 > HB-1 > CB)

The maximum deviation between experimental and numerical ultimate loads remained within approximately 5%, which is considered highly acceptable for nonlinear reinforced concrete simulations. The strong correlation validates the adopted LS-DYNA material models and contact definitions in accurately representing the flexural behavior of HFRP-strengthened RC beams.

5. Conclusion

This study comprehensively investigated the flexural performance of RC beams strengthened with externally bonded HFRP laminates through combined experimental testing and LS-DYNA nonlinear finite element simulation. The results clearly demonstrate that HFRP strengthening significantly enhances load-carrying capacity, stiffness, energy absorption, and moment resistance compared to the unstrengthen control beam. Experimentally, the CB reached an ultimate load of approximately 42 kN, whereas strengthened specimens exhibited substantial improvements. HB-3 achieved approximately 125 kN ($\approx$198% increase), while the anchored specimen HB-5 reached nearly 132 to135 kN ($\approx$214% increase). Moderate laminate thickness improved performance effectively; however, excessive thickness (HB-4) did not produce proportional strength gains due to premature interfacial debonding. This confirms the presence of an optimal laminate thickness beyond which bond efficiency governs structural response rather than laminate tensile capacity alone.

Moment to curvature analysis further verified that HFRP laminates significantly improved rotational capacity. The control beam exhibited an ultimate moment of approximately 17 to18 kN·m, whereas HB-3 and HB-5 reached about 50 to55 kN·m. Energy absorption increased markedly, from 1080 kN·mm for CB to 4580 kN·mm for HB-5, reflecting enhanced deformability and ductile behavior. Cracking stiffness also improved, rising from 10 kN/mm (CB) to 29.5 kN/mm (HB-5). The LS-DYNA simulations showed strong agreement with experimental results, with ultimate load deviations generally within 3 to5%. The numerical model accurately reproduced cracking progression, compressive stress concentration ($\approx$ -39 MPa at the top fiber), strain localization, and displacement profiles (4.8 to 6.2 mm at ultimate state). This validates the suitability of MAT_159 (CSCM) concrete model and contact definitions for simulating externally bonded FRP systems. Overall, HFRP strengthening is highly effective for flexural retrofitting of RC beams, particularly when optimal laminate thickness and adequate anchorage are provided. Bond integrity remains the governing parameter in preventing premature debonding and ensuring full composite action.

5.1 Future Recommendations

Future research should focus on long-term durability performance of HFRP-strengthened beams under cyclic loading, fatigue, temperature variation, and environmental exposure. Parametric studies investigating bond to slip behavior and fracture energy calibration in LS-DYNA are recommended to improve predictive accuracy. Moreover, advanced anchorage systems and hybrid fiber optimization strategies should be explored to maximize strength utilization while preventing interfacial failure. Life-cycle cost and sustainability assessment of hybrid FRP strengthening systems may also provide valuable guidance for large-scale infrastructure rehabilitation applications.

References

Ahmed, A., Zillur Rahman, M., Ou, Y., Liu, S., Mobasher, B., Guo, S., & Zhu, D. (2021). A review on the tensile behavior of fiber-reinforced polymer composites under varying strain rates and temperatures. *Construction and Building Materials*, *294*. https://doi.org/10.1016/j.conbuildmat.2021.123565

Al-Saawani, M. A., Al-Negheimish, A. I., El-Sayed, A. K., & Alhozaimy, A. M. (2022). Finite Element

Modeling of Debonding Failures in FRP-Strengthened Concrete Beams Using Cohesive Zone Model. *Polymers*, *14*(9), 1889. https://doi.org/10.3390/polym14091889

American, & Institute, C. (2017). *440.2R-17: Guide for the Design and Construction of Externally Bonded FRP Systems for Strengthening Concrete Structures*. American Concrete Institute. https://doi.org/10.14359/51700867

ASTM International. (2014). *Test Method for Tensile Properties of Polymer Matrix Composite Materials*. ASTM International. https://doi.org/10.1520/D3039_D3039M-08

ASTM International. (2017). *Test Methods for Flexural Properties of Unreinforced and Reinforced Plastics and Electrical Insulating Materials*. ASTM International. https://doi.org/10.1520/D0790-17

Attari, N., Amziane, S., & Chemrouk, M. (2012). Flexural strengthening of concrete beams using CFRP, GFRP and hybrid FRP sheets. *Construction and Building Materials*, *37*, 746–757. https://doi.org/10.1016/j.conbuildmat.2012.07.052

Bureau of Indian Standards. (2007). *Indian Standard PLAIN AND REINFORCED CONCRETE - CODE OF PRACTICE*. https://law.resource.org/pub/in/bis/S03/is.456.2000.pdf

Bureau of Indian Standards. (2019). *Concrete Mix Design as Per Bureau of Indian Standards*. https://archive.org/details/gov.in.is.10262.2019/mode/2up

Diniță, A., Ripeanu, R. G., Ilincă, C. N., Cursaru, D., Matei, D., Naim, R. I., Tănase, M., & Portoacă, A. I. (2023). Advancements in Fiber-Reinforced Polymer Composites: A Comprehensive Analysis. *Polymers*, *16*(1), 2. https://doi.org/10.3390/polym16010002

Fayed, S., Mansour, W., Tawfik, T. A., Sabol, P., & Katunský, D. (2023). Techniques Used for Bond Strengthening of Sub-Standard Splices in Concrete: A Review Study. *Processes*, *11*(4), 1119. https://doi.org/10.3390/pr11041119

Hassan, A., & Oudah, F. (2024). RF-DYNA — Software for optimized random finite element simulation using LS-DYNA. *Advances in Engineering Software*, *196*, 103724. https://doi.org/10.1016/j.advengsoft.2024.103724

Hawileh, R. A., Rasheed, H. A., Abdalla, J. A., & Al-Tamimi, A. K. (2014). Behavior of reinforced concrete beams strengthened with externally bonded hybrid fiber reinforced polymer systems. *Materials & Design*, *53*, 972–982. https://doi.org/10.1016/j.matdes.2013.07.087

Jafari, A., Shahmansouri, A. A., & Akbarzadeh Bengar, H. (2025). Hybrid CFRP-GFRP sheets for flexural strengthening of continuous RC beams: Experimentation and analytical modeling. *Structural Concrete*, *26*(1), 972–993. https://doi.org/10.1002/suco.202400264

Li, B., Zeng, L., Guo, X., Wang, Y., & Deng, Z. (2022). Flexural Behavior of Full-Scale Damaged Hollow RC Beams Strengthened with Prestressed SCFRP Plate under Four-Point Bending. *Polymers*, *14*(14), 2939. https://doi.org/10.3390/polym14142939

Lin, B., Chun, Q., & Mi, Z. (2024). Flexural behavior of historical RC beams strengthened with hybrid FRP sheets. *Case Studies in Construction Materials*, *20*, e03410. https://doi.org/10.1016/j.cscm.2024.e03410

Lin, H., Hong, W., Yang, Z., Xu, Z., Wang, Y., & Li, B. (2024). Deflection estimation of reinforced concrete beams using long-gauge optic sensors. *Structures*, *69*, 107249. https://doi.org/10.1016/j.istruc.2024.107249

Luo, Z., Wang, H., Ng, C.-T., Fu, J., Zhang, Z., & Wang, C. (2024). On the low-velocity impact properties of CFRP/HAFRP interlayer hybrid fibre composite laminates. *Engineering Structures*, *315*, 118387. https://doi.org/10.1016/j.engstruct.2024.118387

Odusote, J. K., Shittu, W., Adeleke, A. A., Ikubanni, P. P., & Adeyemo, O. (2019). Chemical and Mechanical Properties of Reinforcing Steel Bars from Local Steel Plants. *Journal of Failure Analysis and Prevention*, *19*(4), 1067–1076. https://doi.org/10.1007/s11668-019-00695-x

Palacios-Munoz, B., López-Mesa, B., & Gracia-Villa, L. (2019). Influence of refurbishment and service life of reinforced concrete buildings structures on the estimation of environmental impact. *The International Journal of Life Cycle Assessment*, *24*(11), 1913–1924. https://doi.org/10.1007/s11367-019-01622-w

Pawlak, A. M., Górny, T., Dopierała, Ł., & Paczos, P. (2022). The Use of CFRP for Structural Reinforcement—Literature Review. *Metals*, *12*(9), 1470. https://doi.org/10.3390/met12091470

Sakar, G., Hawileh, R. A., Naser, M. Z., Abdalla, J. A., & Tanarslan, M. (2014). Nonlinear behavior of shear deficient RC beams strengthened with near surface mounted glass fiber reinforcement under cyclic

loading. *Materials & Design*, *61*, 16–25. https://doi.org/10.1016/j.matdes.2014.04.064

Shi, X. (2025). Leveraging emerging technologies to address the crisis of aging concrete infrastructure. *Journal of Infrastructure Preservation and Resilience*, *6*(1), 44. https://doi.org/10.1186/s43065-025-00147-x

Silva, G. H. C., & Meddaikar, Y. (2020). Lamination Parameters for Sandwich and Hybrid Material Composites. *AIAA Journal*, *58*(10), 4604–4611. https://doi.org/10.2514/1.J059093

Tefera, G., Adali, S., & Bright, G. (2024). Flexural failure properties of fiber-reinforced hybrid laminated beam subject to three-point bending. *Scientific Reports*, *14*(1), 9792. https://doi.org/10.1038/s41598-024-60078-7

Yuvaraj, S., Chithra, K., Nirmalkumar, K., & Jeyanth, B. (2023). Performance evaluation of hybrid fibers strengthened reinforced concrete. *Materials Today: Proceedings*. https://doi.org/10.1016/j.matpr.2023.03.667

Zhang, L., Pan, L., Gao, J., Zhang, H., Zhao, L., & Li, C. (2025). Research on hybrid effect of hybrid fiber reinforced plastics: A review. *Journal of Reinforced Plastics and Composites*. https://doi.org/10.1177/07316844251406671